

Deep Switching State Space Model for Nonlinear Time Series Forecasting with Regime Switching

Xiuqin Xu, Hanqiu Peng, and Ying Chen

Abstract—Modern time series data often display complex nonlinear dependencies along with irregular regime-switching behaviors. These features present technical challenges in modeling, inference, and in offering insightful understanding into the underlying stochastic phenomena. To tackle these challenges, we introduce a novel modeling framework known as the Deep Switching State Space Model (DS³M). This framework is engineered to make accurate forecasts for such time series while adeptly identifying the irregular regimes hidden within the dynamics. These identifications not only have significant economic ramifications but also contribute to a deeper understanding of the underlying phenomena. In DS³M, the architecture employs discrete latent variables to represent regimes and continuous latent variables to account for random driving factors. By melding a Recurrent Neural Network (RNN) with a nonlinear Switching State Space Model (SSSM), we manage to capture the nonlinear dependencies and irregular regime-switching behaviors, governed by a Markov chain and parameterized using multilayer perceptrons. We validate the effectiveness and regime identification capabilities of DS³M through short- and long-term forecasting tests on a wide array of simulated and real-world datasets, spanning sectors such as healthcare, economics, traffic, meteorology, and energy. Experimental results reveal that DS³M outperforms several state-of-the-art models in terms of forecasting accuracy, while providing meaningful regime identifications.

Index Terms—Time Series Forecasting; Nonlinear State Space Models; Deep Learning; Stochastic Regime-Switching; Recurrent Neural Networks (RNNs); Interpretable Machine Learning

I. INTRODUCTION

In many studies, researchers face challenges in modeling and inferring from modern time-series data collected across various disciplines. Examples include healthcare (such as sleep apnea), economics (unemployment rates), traffic and transportation (metro passenger volume), meteorology (sea surface temperature), and energy (electricity demand), among others. In these contexts, the conventional assumptions of linearity, normality, and stationarity that often form the foundation of statistical modeling are frequently inadequate. They give way to complex nonlinear dynamics intertwined with irregular regime shifts. We show that in these settings, both conventional statistical models and standard deep learning approaches suffer from either a severe modeling misspecification or a lack of effective identification of meaningful stochastic regimes. Given the criticality of such regime identification, not only

Xiuqin Xu is with McKinsey, Singapore 048583 (email: xiuqin.sherry.xu@gmail.com)

Hanqiu Peng is with the Department of Mathematics, National University of Singapore, Singapore 119076 (email: penghanqiu@u.nus.edu)

Ying Chen is with the Department of Mathematics, Asian Institute of Digital Finance, and Risk Management Institute, National University of Singapore, Singapore 117602 (email: matcheny@nus.edu.sg)

for its economic implications but also for the profound comprehension of underlying phenomena, we propose a novel solution – the Deep Switching State Space Model (DS³M). This framework is tailored to simultaneously provide efficient inference and a meaningful interpretation of these complex dynamics in a computationally tractable manner.

This type of time series often relies on certain unobservable (latent) regime states. For instance, the unemployment rate is influenced by economic conditions like booms or recessions. It is also affected by latent continuous variables, such as regional wage elasticity, which vary with the discrete regime states. Deciphering these discrete and continuous latent variables accurately can offer significant insights into the nonlinear time series characterized by stochastic regime-switching. To conduct a thorough analysis, we need to address the two challenges mentioned earlier: modeling misspecification and the absence of meaningful identification of the stochastic regimes.

The misspecification occurs when the assumed dynamics cannot accurately represent the actual behaviors of the time series. Given the presence of regimes within time series data, Switching State Space Models (switching SSMs) are arguably the most widely used. In these models, the evolution of the time series is presumed to be driven by hidden factors that switch among discrete regimes, see [1]–[4]. Specifically, the switching SSM generalizes Hidden Markov Models (HMMs) and State Space Models (SSMs), where the dynamics within each regime are typically represented by simple linear models that can be efficiently estimated even with a limited sample size [5], while the transitions between regimes are governed by the hidden transition probabilities of a Markov chain. By extending the local linear models to encompass various regimes, the resulting model aims to approximate globally nonlinear behavior while maintaining interpretability. For complex dependence where the stage-wise linear structure is insufficient, SSMs can be customized with certain pre-specified nonlinear transition and/or emission functions [6]. Despite their popularity, existing nonlinear models rely on predetermined local parametric forms with simple structures, either linear or nonlinear, which may be insufficient to describe the actual patterns in modern nonlinear time series.

On the contrary, the field of deep learning and especially recurrent neural networks with gate structures, such as the Long-Short Term Memory (LSTM, [7]), Gated Recurrent Unit (GRU, [8]), Transformers [9], and temporal convolution networks [10], have emerged as the new benchmark to model nonlinear time series with highly complex dependencies. However, the relatively small sample size of real

data, and more importantly, the stochastic behaviors of regime switching, make standard deep learning approaches computationally infeasible and lack interpretation on the fitted models. Moreover, the classic deep learning models are deterministic and ignore the presence of unobserved stochastic signals in the dynamic system. The only randomness allowed appears in the conditional output probability models, with either a simple unimodal distribution, e.g. Gaussian in [11], or a mixture of simple unimodal distributions, e.g. Gaussian Mixture models in [12]. Since it is ambitious for a model with deterministic structures to capture the stochastic behavior in nonlinear time series with non-stationary patterns/transitions [13], it has to require a large number of parameters to ensure a reasonable modeling accuracy. In other words, the remedy needs a large sample size for consistent estimation, which unfortunately is unrealistic as the amount of real-world time series data is usually not that big in many disciplines.

This has advocated the integration of deep learning and stochastic latent variable models to leverage their complementary strengths of nonlinear representation and interpretability [14]–[16]. Deep SSMs introduce continuous Gaussian latent variables at each time step to represent a latent continuous random variable [17]–[22]. In [23], a recurrent neural network is combined with a continuous-discrete Kalman filter (SSM) to model time series with irregular intervals. These models can be viewed as sequences of variational auto-encoders. While powerful in terms of accuracy, interpreting nonlinear dynamics becomes challenging as there is no knowledge of discrete regimes. The other type of deep SSMs incorporates discrete latent variables for the interpretation of regime switching [24]–[26], where the evolution of time series is solely driven by the discrete latent variable. Such a setting either deviates from reality or limits its applicability, as it disregards the coexistence of both discrete and continuous latent variables.

We propose a Deep Switching State Space Model (DS^3M) for performing interpretable and efficient inference on nonlinear time series characterized by irregular regime switching. This framework is engineered to make accurate forecasts for such time series while adeptly identifying the irregular regimes hidden within the dynamics. These identifications not only have significant economic ramifications but also contribute to a deeper understanding of the underlying phenomena. In DS^3M , the architecture employs discrete latent variables to represent regimes and continuous latent variables to account for random driving factors. It comprises a Recurrent Neural Network (RNN) and a Nonlinear Switching State Space Model (SSSM), where emission and transition functions are governed by a Markov chain of the discrete latent variables and parameterized by multilayer perceptrons. These discrete latent variables are assumed to influence both the observed time series and the values of continuous latent variables. In essence, regime switching has a direct impact on the time series and an indirect influence via its effect on the continuous latent variables. The RNN and SSSM are integrated to allow the continuous latent variables in the SSSM to benefit from the long-term information captured by the RNN. Furthermore, the RNN is skip-connected to the observations to enhance forecasting accuracy.

We have developed an approximate variational inference algorithm that can scale to large data sets. The key idea involves marginalizing the discrete latent variables solely at each time step and subsequently utilizing a reparametrization trick for the continuous latent variables. This method has been applied to enable short- and long-term forecasting across a range of simulated and real datasets spanning various domains such as healthcare, economics, traffic, meteorology, and energy. It shows that the proposed model can leverage the interpretability of discrete latent variables, the powerful representation ability of continuous latent variables, and the nonlinearity characteristic of deep learning models. Across most scenarios, DS^3M achieves superior performance compared to several state-of-the-art methods (e.g. GRU, SRNN [18], DSARF [27] and SNLDS [28]), while also demonstrating the meaningful identification of discrete latent variables and enhanced predictive accuracy. Notably, the learned regimes' duration in DS^3M tends to be longer than the alternatives, aligning more closely with empirical observations in contrast to the chaotic and frequent switching identified in alternative methods.

We build upon methods developed by [28]. Many aspects of the current paper, including our proposed modeling framework, designed architecture, and generality beyond Markov dependence, are novel in relation to that prior work. Specifically, DS^3M incorporates both discrete and continuous latent variables, enabling a comprehensive understanding of the joint impact of regimes and stochastic signals on the evolution of nonlinear time series. The deep learning architecture is tailored to mirror the inherent dependence structure present in real-world time series, considering factors like the endogeneity between the two types of latent variables. Unlike [28], where the approximated posterior of continuous latent variables does not depend on discrete latent variables, we employ connected inference structures that mimic true posterior relationships to mitigate the posterior collapse problem of discrete latent variables. In the current context, we extend State Space Models (SSMs) with hidden variables representing more than one-step temporal dependence through recurrent networks. This approach allows us to address non-Markov problems within the Markov framework.

Our paper contributes a recipe for employing statistical modeling and deep learning to achieve interpretable inference for modern time series with complex dynamics. By introducing both continuous and discrete latent variables in the recurrent neural network, we efficiently harness the potent representation capabilities of continuous latent variables to capture rich dependence and enable economically meaningful identifications of discrete latent variables. The novel amortized variational inference method renders it suitable for both small and large datasets. When applied to a variety of simulated and real data across various disciplines, we showcase the robust competitive performance of DS^3M compared to state-of-the-art technologies.

The rest of the paper is organized as follows. Section II reviews the related works. Section III details the proposed DS^3M and the scalable inference algorithm. Section IV presents the numerical performance of the DS^3M with several simulated

and six real-world data sets in different disciplines. Section V concludes. Data and codes can be found on the Github website.

II. BACKGROUND AND RELATED WORKS

Denote a time series of T observations as $y_{1:T} = \{y_1, y_2, \dots, y_T\}$, $y_t \in \mathbb{R}^D$ and a sequence of inputs as $x_{1:T} = \{x_1, x_2, \dots, x_T\}$, $x_t \in \mathbb{R}^U$. In the setting of time series forecasting, x_t can be one or multiple lagged values of the time series, e.g. y_{t-1} and higher orders y_{t-2}, y_{t-3}, \dots . The inputs x_t could also contain exogenous variables. We are interested in modeling $p(y_{1:T}|x_{1:T})$.

In the class of switching SSMs, the simplest form is the switching linear dynamical system (SLDS), where the dynamics of each regime is explained by a linear state space model. The discrete latent variables, denoted as $d_t \in \{1, 2, \dots, K\}$ at each time step $t = 1, 2, \dots, T$, follows a Markov chain. In particular, $d_t|d_{t-1}$ is assumed to follow a transition matrix $\Gamma \in R^{K \times K}$, where $\Gamma_{i,j} = p(d_t = j|d_{t-1} = i)$. The discrete latent variables d_t have impact on both the continuous latent variables $z_t \in \mathbb{R}^Z$ and y_t through the following transition and emission functions:

$$z_t = W_z^{(d_t)} z_{t-1} + W_x^{(d_t)} x_t + b_z^{(d_t)} + e_t, e_t \sim N(0, \Sigma_z^{(d_t)}) \quad (1)$$

$$y_t = W_y^{(d_t)} z_t + b_y^{(d_t)} + \epsilon_t, \epsilon_t \sim N(0, \Sigma_y^{(d_t)}) \quad (2)$$

where $W_z^{(d_t)} \in \mathbb{R}^{Z \times Z}$, $W_x^{(d_t)} \in \mathbb{R}^{Z \times U}$, $b_z^{(d_t)} \in \mathbb{R}^{Z \times 1}$, $\Sigma_z^{(d_t)} \in \mathbb{R}^{Z \times Z}$, $W_y^{(d_t)} \in \mathbb{R}^{D \times Z}$, $b_y^{(d_t)} \in \mathbb{R}^{D \times 1}$ and $\Sigma_y^{(d_t)} \in \mathbb{R}^{D \times D}$. The **transition** function in (1) determines the evolution of the latent variable. The **emission** function in (2) specifies the dynamics of the observed time series, given the state of the latent variables at time t . The transition noise e_t and emission noise ϵ_t are Gaussian distributed. When $K = 1$, the model is also termed as the Linear Gaussian State Space Model (LGSSM).

There have been several extensions to the SLDS by introducing nonlinear structures. The RSSSM is proposed in [6] which adopts a pre-specified nonlinear transition function. The SVAE model [24] parametrizes the emission function by neural networks, while the transition function remains linear. The SNLDS model [28] parametrizes both the emission and transition functions with nonlinear neural networks. The DSARF [27] approximates high-dimensional time series with a multiplication of latent factors and latent weights, where the latent weights are modeled by a nonlinear autoregressive model, switched by a Markov chain of discrete latent variables. Most of the above-mentioned work assumed that the d_t only influences the transition of z_t . Our work, on the other hand, assumes that the d_t which represents the long-term dynamic changes of the time series, affects both y_t and z_t .

The discrete switching variables in the SLDS are assumed to be Markov, i.e. d_t depends on d_{t-1} only. The recurrent SLDS (rSLDS) proposed in [29] and [30] extends the open-loop Markov dynamics and makes d_t depending on the hidden state z_{t-1} . In [31], a tree structure prior is imposed on the switching variables of rSLDS, where the dynamics of the switching variables behave similarly in the same subtrees. The deep Rao-Blackwellised Particle Filter proposed in [32]

also allow d_t to depend on z_{t-1} . The SNLDS model [28] extends the open-loop Markov dynamics by making d_t depends on last observations. Such recurrent structures serve as a presence of disturbance to the switching dynamics. Although such recurrent structures sometimes can improve the accuracy, they can also lead to unnecessarily frequent state shifts in the estimated discrete latent variables, making interpretations difficult, see our simulated toy example. There is a need for a well-designed architecture that allows the disturbance to be reasonably represented, and simultaneously does not lead to over frequently switching. In this work, we stick to a Markov dynamic of the discrete latent variable and push the non-Markov dynamics into the continuous latent variables that depend on the hidden states of a recurrent neural network summarizing the information coming from the past.

There is a common question in the switching models, i.e. to decide the number of switching states. In [2], a hierarchical Dirichlet process prior is imposed on the switching variables. The model in [33] directly outputs the parameters for the SSMs at each time step via RNN, and this model can be viewed as switching SSM with an infinite number of switching states. Most works, including this work, assume that the number of states is fixed with prior knowledge. The discrete latent variable can also be modeled as a Semi-Markov chain, where the duration of each state is controlled by another discrete random variable, see [25], [26], [34].

III. DEEP SWITCHING STATE SPACE MODEL (DS³M)

In this section, we will detail the generative and inference network of the DS³M.

a) Generative network: The generating procedure of the DS³M contains four steps.

(1) At time step t , a forward RNN is used to process the input data: $h_t = f_h(h_{t-1}, x_t)$, where h_t is the RNN hidden state and f_h can be an LSTM or GRU.

(2) The discrete latent variable $d_t \in \{1, \dots, K\}$ evolves following a Markov transition matrix $\Gamma \in R^{K \times K}$ with $\Gamma_{i,j} = p(d_t = j|d_{t-1} = i)$. Here K refers to the number of regimes states.

(3) The transition of the continuous latent variable z_t is determined by d_t as follows:

$$z_t|z_{t-1}, h_t, d_t = k \sim N(\mu_t^{(k)}, \Sigma_t^{(k)}), \\ \mu_t^{(k)} = f_1^{(k)}(z_{t-1}, h_t), \quad \log \Sigma_t^{(k)} = f_2^{(k)}(z_{t-1}, h_t),$$

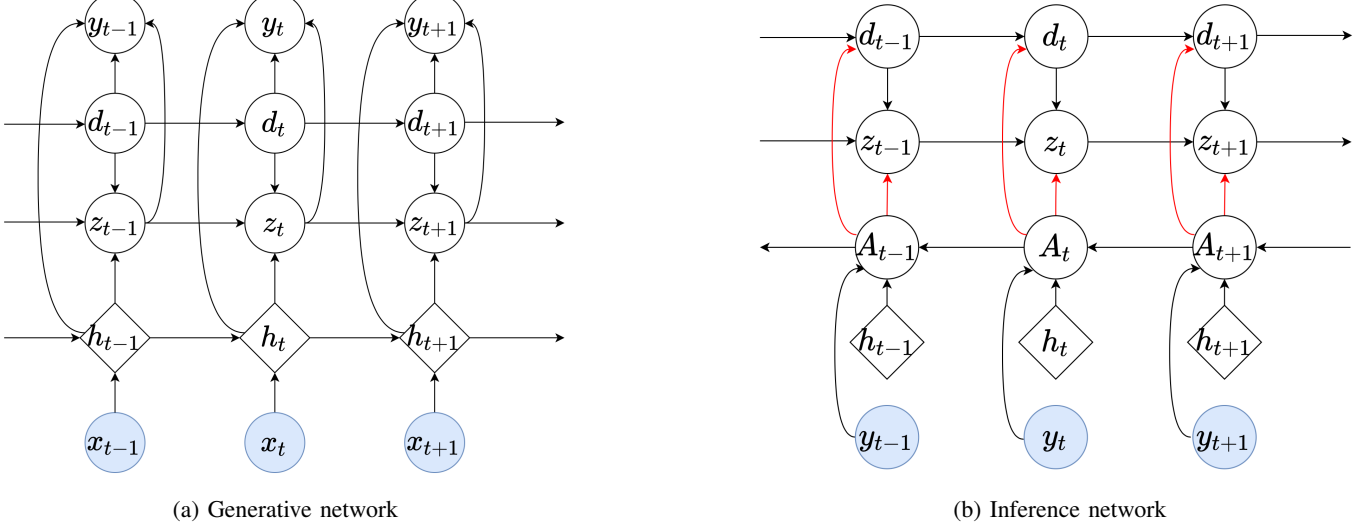
where the mean $\mu_t^{(k)}$ and the diagonal covariance matrix $\Sigma_t^{(k)}$ are represented with neural network models $f_1^{(k)}$ and $f_2^{(k)}$.

(4) The time series y_t is then modeled as

$$y_t|z_t, h_t, d_t = k \sim \pi(\Phi_t^{(k)}), \quad \Phi_t^{(k)} = f_o^{(k)}(z_t, h_t),$$

where π represents the output probabilistic model with parameter $\Phi_t^{(k)}$ given by the neural network model $f_o^{(k)}$. The choice of π depends on the stochastic behavior of the observed time series, e.g. Gaussian for data with bell shape or lognormal for asymmetric data.

Figure 1a displays a graphical representation of the DS³M. It is important to stress the key differences between DS³M

Fig. 1: Deep Switching State Space Model (DS³M)

and the state-of-the-art SNLDS. We stack an RNN below the SSSM and design a direct connection of the hidden state h_t to the time series y_t inspired by the skip connection in ResNet [35], Transformers [36] and SRNN [18]. From a modeling aspect, a lack of this connection will force the continuous latent variable z_t to encode all the relevant continuous information. The connection between y_t and h_t on the other hand allows a clear structure, where both the deterministic hidden states and the stochastic latent variables can separately encode different aspects of information. The addition of the RNN and the skip connection is important as we aim at out-of-sample prediction task, while the focus of SNLDS is the segmentation of time series, i.e. identify the regimes (in-sample inference).

Denote $\theta = \{f_h, \Gamma, \{f_1^{(k)}\}_{k=1}^K, \{f_2^{(k)}\}_{k=1}^K, \{f_o^{(k)}\}_{k=1}^K\}$ as the parameters of the DS³M. The joint probability is represented as

$$\begin{aligned} p_\theta(\mathbf{y}_{1:T}, \mathbf{z}_{1:T}, \mathbf{d}_{1:T} | \mathbf{x}_{1:T}) \\ = \prod_{t=1}^T p_\theta(\mathbf{y}_t | \mathbf{z}_t, \mathbf{h}_t, \mathbf{d}_t) p_\theta(\mathbf{z}_t | \mathbf{z}_{t-1}, \mathbf{h}_t, \mathbf{d}_t) p_\theta(\mathbf{d}_t | \mathbf{d}_{t-1}). \end{aligned} \quad (3)$$

Given the non-linearity introduced by neural networks, it is intractable to obtain the likelihood of observations, denoted by $\mathcal{L}(\theta)$, by averaging out $\mathbf{z}_{1:T}$ and $\mathbf{d}_{1:T}$ in (3). In other words, the maximum likelihood method is not practically useful. We develop a scalable learning and inference algorithm for the DS³M using variational inference. Specifically, we design an inference network with parameter ϕ to approximate the posterior $p(\mathbf{z}_{1:T}, \mathbf{d}_{1:T} | \mathbf{x}_{1:T}, \mathbf{y}_{1:T})$ and then optimize an evidence lower bound based on this approximated posterior.

b) Inference network: In the inference network, we maximize a variational evidence lower bound $\text{ELBO}(\theta, \phi) \leq \mathcal{L}(\theta)$ with respect to both θ and ϕ , where

$$\begin{aligned} \text{ELBO}(\theta, \phi) \\ = \mathbb{E}_{q_\phi} [\log p_\theta(\mathbf{y}_{1:T} | \mathbf{z}_{1:T}, \mathbf{d}_{1:T}, \mathbf{x}_{1:T})] \\ - \text{KL}(q_\phi(\mathbf{z}_{1:T}, \mathbf{d}_{1:T} | \mathbf{y}_{1:T}, \mathbf{x}_{1:T}) \| p_\theta(\mathbf{z}_{1:T}, \mathbf{d}_{1:T} | \mathbf{x}_{1:T})). \end{aligned}$$

The ELBO is tight, i.e. $\mathcal{L}(\theta) = \text{ELBO}(\theta, \phi)$, only when the approximated posterior $q_\phi(\mathbf{z}_{1:T}, \mathbf{d}_{1:T} | \mathbf{y}_{1:T}, \mathbf{x}_{1:T})$ is equal to

the true posterior $p_\theta(\mathbf{z}_{1:T}, \mathbf{d}_{1:T} | \mathbf{y}_{1:T}, \mathbf{x}_{1:T})$, which is unfortunately intractable. To achieve a tight ELBO, we consider the following factorization derived from the d-separation [37] according to the generative network:

$$\begin{aligned} p_\theta(\mathbf{z}_{1:T}, \mathbf{d}_{1:T} | \mathbf{y}_{1:T}, \mathbf{x}_{1:T}) \\ = \prod_t p_\theta(\mathbf{z}_t | \mathbf{z}_{t-1}, \mathbf{d}_t, \mathbf{y}_{t:T}, \mathbf{h}_{t:T}) p_\theta(\mathbf{d}_t | \mathbf{d}_{t-1}, \mathbf{y}_{t:T}, \mathbf{h}_{t:T}), \end{aligned}$$

where the posterior of $\mathbf{z}_t, \mathbf{d}_t$ depends on the past information encoded in $\{\mathbf{z}_{t-1}, \mathbf{d}_{t-1}\}$ as well as the future information in $\{\mathbf{y}_{t:T}, \mathbf{h}_{t:T}\}$. The inference is designed to use the information from all time steps to approximate the posterior at each time step t :

$$\begin{aligned} q_\phi(\mathbf{z}_{1:T}, \mathbf{d}_{1:T} | \mathbf{y}_{1:T}, \mathbf{x}_{1:T}) \\ = \prod_t q_{\phi_z}(\mathbf{z}_t | \mathbf{z}_{t-1}, \mathbf{d}_t, \mathbf{A}_t) q_{\phi_d}(\mathbf{d}_t | \mathbf{d}_{t-1}, \mathbf{A}_t), \end{aligned} \quad (4)$$

where $\mathbf{A}_t = g_{\phi_A}(\mathbf{A}_{t+1}, [\mathbf{y}_t, \mathbf{h}_t])$ and $\phi = \{\phi_z, \phi_d, \phi_A\}$. We parameterize g_{ϕ_A} as a backward RNN and $q_{\phi_z}(\mathbf{z}_t | \mathbf{z}_{t-1}, \mathbf{d}_t, \mathbf{A}_t)$ with a Gaussian probabilistic density:

$$\begin{aligned} \mathbf{z}_t | \mathbf{z}_{t-1}, \mathbf{d}_t = k, \mathbf{A}_t &\sim N(\mu_t^{(k)}, \Sigma_t^{(k)}), \\ \mu_t^{(k)} &= g_1^{(k)}(z_{t-1}, \mathbf{A}_t), \quad \log \Sigma_t^{(k)} = g_2^{(k)}(z_{t-1}, \mathbf{A}_t), \end{aligned}$$

where \mathbf{z}_t is a Gaussian variable with mean $\mu_t^{(k)}$ and diagonal variance matrix $\Sigma_t^{(k)}$ determined by neural network models $g_1^{(k)}$ and $g_2^{(k)}$. Moreover, $q_{\phi_d}(\mathbf{d}_t | \mathbf{A}_t, \mathbf{d}_{t-1})$ is parameterized as a Categorical distribution:

$$\mathbf{d}_t | \mathbf{A}_t, \mathbf{d}_{t-1} = k \sim \text{Cat}(\text{softmax}(W^{(k)} \mathbf{A}_t)).$$

The graphical model of the inference network is shown in Figure 1b. In addition, we have

$$p_\theta(\mathbf{z}_{1:T}, \mathbf{d}_{1:T} | \mathbf{x}_{1:T}) = \prod_t p_\theta(\mathbf{d}_t | \mathbf{d}_{t-1}) p_\theta(\mathbf{z}_t | \mathbf{z}_{t-1}, \mathbf{d}_t, \mathbf{h}_t).$$

With the defined approximate posterior, the ELBO can be derived as follows:

$$\begin{aligned}
& \text{ELBO}(\theta, \phi) \\
&= \sum_t \left\{ \mathbb{E}_{q_\phi^*}(\mathbf{z}_{t-1}, \mathbf{d}_{t-1}) \sum_{\mathbf{d}_t} q_{\phi_d}(\mathbf{d}_t) \mathbb{E}_{q_{\phi_z}(\mathbf{z}_t)} [\log p_\theta(\mathbf{y}_t | \mathbf{z}_t, \mathbf{d}_t, \mathbf{h}_t)] - \right. \\
& \quad \mathbb{E}_{q_\phi^*}(\mathbf{z}_{t-1}, \mathbf{d}_{t-1}) \sum_{\mathbf{d}_t} q_{\phi_d}(\mathbf{d}_t) \text{KL} [q_{\phi_z}(\mathbf{z}_t | \mathbf{z}_{t-1}, \mathbf{d}_t, \mathbf{A}_t) \| p_\theta(\mathbf{z}_t | \mathbf{z}_{t-1}, \mathbf{d}_t, \mathbf{h}_t)] \\
& \quad \left. - \mathbb{E}_{q_\phi^*}(\mathbf{d}_{t-2}) \sum_{\mathbf{d}_{t-1}} q_{\phi_d}(\mathbf{d}_{t-1}) \text{KL} [q_{\phi_d}(\mathbf{d}_t | \mathbf{d}_{t-1}, \mathbf{A}_t) \| p_\theta(\mathbf{d}_t | \mathbf{d}_{t-1})] \right\},
\end{aligned}$$

where $q_\phi^*(\mathbf{z}_t, \mathbf{d}_t) = \int q_\phi(\mathbf{z}_{1:t}, \mathbf{d}_{1:t} | \mathbf{y}_{1:T}, \mathbf{x}_{1:T}) d\mathbf{z}_{1:t-1} d\mathbf{d}_{1:t-1}$ and $q_\phi^*(\mathbf{d}_t) = \int q_{\phi_d}(\mathbf{d}_{1:t} | \mathbf{y}_{1:T}, \mathbf{x}_{1:T}) d\mathbf{d}_{1:t-1}$. We approximate the ELBO using a Monte Carlo method. Specifically, we sample $(z_t^{(s)}, d_t^{(s)})$ for $t = 1, \dots, T$ from $q_\phi^*(\mathbf{z}_t, \mathbf{d}_t)$ using ancestral sampling according to (4) and approximate ELBO as follows:

$$\begin{aligned}
& \text{ELBO}(\theta, \phi) \\
& \approx \sum_t \left\{ \sum_{\mathbf{d}_t} q_{\phi_d}(\mathbf{d}_t) \log p_\theta(\mathbf{y}_t | \mathbf{z}_t^{(s)}, \mathbf{d}_t, \mathbf{h}_t) \right. \\
& \quad \left. - \sum_{\mathbf{d}_t} q_{\phi_d}(\mathbf{d}_t) \text{KL} [q_{\phi_z}(\mathbf{z}_t | \mathbf{z}_{t-1}^{(s)}, \mathbf{d}_t, \mathbf{A}_t) \| p_\theta(\mathbf{z}_t | \mathbf{z}_{t-1}^{(s)}, \mathbf{d}_t, \mathbf{h}_t)] \right. \\
& \quad \left. - \sum_{\mathbf{d}_{t-1}} q_{\phi_d}(\mathbf{d}_{t-1}) \text{KL} [q_{\phi_d}(\mathbf{d}_t | \mathbf{d}_{t-1}, \mathbf{A}_t) \| p_\theta(\mathbf{d}_t | \mathbf{d}_{t-1})] \right\}.
\end{aligned} \tag{5}$$

It is easy to obtain $\nabla_\theta \text{ELBO}(\theta, \phi)$, while it is not the case for $\nabla_\phi \text{ELBO}(\theta, \phi)$, as ϕ also appears in the expectation. The score function gradient estimator [38] can be used to approximate the gradient, but the obtained results suffer from high variance. Thus the reparameterization approach is often used to reduce the variance [14], [15]. We apply the reparameterization approach to the continuous latent variable z_t in the ELBO. The gradients can then be backpropagated through the continuous random variables. One could not use the Gumble-softmax reparameterization trick for the discrete latent variables as non-integer values of d_t are invalid for our generative model. Also, in [28], it shows that using the Gumble-softmax reparameterization trick will reduce the benefit of discrete latent variables. As an alternative approach, in (5), we marginalize out the discrete variable d_t with a summation over its probability at each time step t , and do not marginalize out the discrete variable before time t . This introduces a biased gradient estimator for ϕ_d and ϕ_z and it can be viewed as gradient clips where the gradients from the previous time steps are ignored. In our experiments, such an approximation performs very well compared to the unbiased score function estimator and we consider the bias ignorable. We have done some experiments that marginalized more than one step in (5). The performance is similar, but the time complexity in computing (5) will increase from $O(KT)$ to $O(K^2T)$. Therefore, we stick to the current setting.

A summary of the structured inference algorithm is given in Algorithm 1.

Algorithm 1 Structured Inference Algorithm for DS³M

Inputs: $\{x_{1:T}\}_{i=1}^N, \{y_{1:T}\}_{i=1}^N$, randomly initialized $\phi^{(0)}$ and $\theta^{(0)}$
Outputs: θ, ϕ
while $Iter < M$ **do**
 1. Sample a mini-batch sequences $\{x_{1:T}\}_{i=1}^B, \{y_{1:T}\}_{i=1}^B$ from the dataset
 2. Generate $z_t^{(s)}, d_t^{(s)}$ for $t = 1, 2, \dots, T$ sequentially according to (4) to approximate the ELBO in (5)
 3. Derive $\nabla_\theta \text{ELBO}(\theta, \phi)$ and $\nabla_\phi \text{ELBO}(\theta, \phi)$
 4. Update $\theta^{(Iter)}, \phi^{(Iter)}$ using the ADAM, set $Iter = Iter + 1$
end while

It is worth mentioning that the SNLDS marginalizes the discrete latent variables using the exact posterior derived with the forward-backward algorithm, while the DS³M marginalizes the discrete latent variables using the approximate posterior at each time step. One potential problem of marginalizing the discrete latent variables using the exact posterior is that the approximate posterior for z_t does not depend on d_t anymore. This could lead to a severe posterior collapse problem that d_t is not used at all. They proposed an entropy regularizer to encourage an evenly distributed posterior for d_t . However, there is no guarantee that an evenly distributed posterior will produce meaningful interpretation. In contrast, we use a approximated posterior of z_t that depends on d_t to form connected inference between z_t and d_t . The posterior collapse problem for the discrete latent variables does not appear in our experiments.

We demonstrate the presence of stability and convergence in DS³M.

Theorem 1: Under certain conditions, for the neural networks $f_1^{(k)}$ and $f_2^{(k)}$ that parameterize the mean $\mu_t^{(k)}$ and diagonal covariance matrix $\Sigma_t^{(k)}$ of the latent state dynamics $z_t \sim \mathcal{N}(\mu_t^{(k)}, \Sigma_t^{(k)})$ using arbitrary activation functions, there exists an equivalent pointwise affine map that ensures global mean-square stability of the latent variable z_t .

We provide a detailed proof in the Appendix. Moreover, in accordance with the convergence theory for deep neural networks and recurrent neural networks proposed by Zeyuan Allen-Zhu et al. [39], DS³M converges initialized with random Gaussian values and trained using Stochastic Gradient Descent (SGD).

c) Predictive distributions: Given a trained model, we are interested in the predictive distributions for the one-step-ahead to τ -step-ahead observations $\{y_{T+1}, \dots, y_{T+\tau}\}$ and the discrete latent variables $\{d_{T+1}, \dots, d_{T+\tau}\}$. We first make inference on the posterior distributions of $\{z_t, d_t\}_{t=1}^T$ and then generate samples of $\{z_t^{(s)}, d_t^{(s)}, y_t^{(s)}\}_{t=T}^{T+\tau}, s = 1, \dots, S$ and S represents the number of Monte Carlo samples. The predictive distributions are then approximated with empirical distribution functions of the generated samples.

IV. EXPERIMENTS

In this section, we evaluate DS³M through various experiments. We first consider a simulated 1-dimensional (1-d) time series whose true dynamics follow a nonlinear switching state space model, as well as a simulated 10-dimensional (10-d) time series based on the Lorenz attractor. Furthermore,

we apply DS³M to several real-world datasets spanning diverse applications, such as health care, transportation, energy, and econometrics. Both simulations and real data analyses demonstrate that DS³M effectively captures switching regimes and achieves competitive predictive accuracy when compared with several state-of-the-art methods, including SRNN, GRU, DSARF, and SNLDS. Specifically, SRNN can be considered our model without discrete latent variables. DSARF and SNLDS are two nonlinear dynamic latent variable models for time series that incorporate both continuous and discrete latent variables. DSARF's superior performance over models like rSLDS and SLDS in time series forecasting with similar datasets has been demonstrated [27]. Hence, we omit the comparison to SLDS and rSLDS in the subsequent analysis. To ensure fair comparison, we select the same datasets and employ the official codes of DSARF and SNLDS. Further details about hyperparameters are provided in the supplementary material. For a fair comparison, we select the same data sets and use the official codes of DSARF and SNLDS. Details of the hyperparameters are provided in the supplementary material.

A. Simulations

a) Toy example: For the toy simulated example, we simulated data with a length of 2000 from the following nonlinear switching state space model:

$$\begin{aligned} d_0 &\sim \text{Bernouli}(0.5), z_0 = 0 \\ d_t | d_{t-1} &\sim \Gamma = \begin{bmatrix} 0.95 & 0.05 \\ 0.05 & 0.95 \end{bmatrix}, d_t \in \{0, 1\} \\ Z_{t|d_t=0} &= 0.6Z_{t-1} + 0.4 \times \tanh(X_t + Z_{t-1}) + w_t^{(0)}, \\ Z_{t|d_t=1} &= 0.1Z_{t-1} + 0.2 \times \sin(X_t + Z_{t-1}) + w_t^{(1)}, \\ Y_{t|d_t=0} &= 1.5Z_t + \tanh(Z_t) + v_t^{(0)}, \\ Y_{t|d_t=1} &= 0.5Z_t + \sin(Z_t) + v_t^{(1)}, \\ w_t^{(0)} &\sim N(0, 10), w_t^{(1)} \sim N(0, 1), \\ v_t^{(0)} &\sim N(0, 5), v_t^{(1)} \sim N(0, 0.5) \end{aligned}$$

For the simulated time series, the switching indicator d_t controls both the dynamics of the continuous latent variable z_t and the observation y_t . By design, y_t is much more volatile (has higher variance) when $d_t = 0$ compared with $d_t = 1$. Note that we crafted the Markovian transition matrix with the intention of maintaining a high probability for the regime to remain in its current state, rather than undergoing frequent and chaotic shifts. This deliberate design choice reflects the characteristics often observed in various real-world contexts. Our aim is to closely mimic the realistic settings of these fields, where the relative stability of regimes is a prevalent feature. We transform the times series into subsequences with a length of 20, resulting in 1980 subsequences. The first 1000, the following 480, and the last 500 subsequences are used for training, validation, and testing. We set $x_t = y_{t-1}$.

Figure 2a showcases the one-step-ahead forecasting results (one experiment run) of DS³M for the testing data, along with the predicted switching indicators of DS³M, SNLDS,

and DSARF. Notably, the predictive means of the observations closely align with the actual observations, while the 90% confidence intervals effectively encompass a majority of the data points. Furthermore, DS³M adeptly adapts by offering wider confidence intervals during volatile periods and narrower ones during more stable data phases. Importantly, the learned transition matrix, $\begin{bmatrix} 0.91 & 0.09 \\ 0.18 & 0.82 \end{bmatrix}$, exhibits close alignment with the true transition matrix.

Table I presents a summary of forecasting and inference accuracy across five experiment runs. DS³M excels with lower forecasting RMSE (Root Mean Square Error) for observations, showing a relative enhancement of 11.46% and 4.41% over SNLDS and DSARF respectively. Furthermore, DS³M achieves significantly higher state prediction accuracy (with a relative improvement of 44.99% compared to SNLDS) and a higher F1 score (with a relative improvement of 41.77% compared to SNLDS) for the switching indicators. While DSARF and DS³M exhibit comparable state prediction accuracy and F1 score, Figure 2a shows that DS³M provides much reliable predictions for switching indicators as compared to the ground truth, while SNLDS and DSARF tend to switch over frequently. The mean duration lengths of the two states in DS³M are 7.509 and 7.634, although they are still smaller than the true values (24 and 24). However, this performance is notably better than the alternatives, where duration lengths range around 1–4. When applied to segmenting time series (inference), DS³M also showcases superior accuracy and F1 scores compared to SNLDS, while performing similarly to DSARF.

b) Lorenz attractor: Lorenz attractor is a canonical nonlinear dynamical system with the following nonlinear dynamic for $z_t = [z_{t,1}, z_{t,2}, z_{t,3}]$:

$$\frac{dz}{dt} = \begin{bmatrix} \alpha(z_2 - z_1) \\ z_1(\beta - z_1) - z_2 \\ z_1z_2 - \gamma z_3 \end{bmatrix}$$

The variable $z_t = [z_{t,1}, z_{t,2}, z_{t,3}]^T$ is treated as a latent variable, and thus is unobservable. In the simulation, we considered a 10-dimensional time series $y_t = Wz_t + v_t$, where $W \in R^{10 \times 3}$, $v_t \sim N(0, 0.5I_{10})$. The same dataset was used in [27]. Similar to the toy example, we set $x_t = y_{t-1}$. The traces of the Lorenz attractor roughly can be separated into two ellipses. We simulated a time series with a length of 3000 and transform the time series into subsequences with a length of 5, resulting in 2990 subsequences. The first 1000, the following 990, and the last 1000 subsequences are used for training, validation, and testing respectively.

The forecasted switching variables of the DS³M are shown in Figure 2b. The model successfully separates the two ellipses with a forecasting accuracy of 0.882 ± 0.079 (a relative improvement of 43.14% and 11.99% compared with SNLDS and DSARF respectively) and an F1 score of 0.837 ± 0.127 (a relative improvement of 39.50% and 8.11%), see Table I. For the forecasting accuracy of the observations, the DS³M has smaller RMSE and MAPE compared to SNLDS, but did not beat DSARF. The superior performance of the DSARF is because that the simulated dataset is generated as a multipli-

TABLE I: Summary of the simulation results (mean \pm standard deviation) over five experiment runs

		Toy			Lorenz		
		DS ³ M	SNLDS	DSARF	DS ³ M	SNLDS	DSARF
Forecasting	RMSE	14.572 \pm 0.352	16.541 \pm 0.024	15.244 \pm 0.136	0.168 \pm 0.017	0.226 \pm 0.065	0.030 \pm 0.000
	Duration for $dt=1$	7.509 \pm 1.579	1.282 \pm 0.001	3.946 \pm 0.426	-	-	-
	Duration for $dt=0$	7.634 \pm 1.667	1.667 \pm 0.012	3.274 \pm 0.985	-	-	-
	Accuracy (%)	0.788 \pm 0.033	0.543 \pm 0.001	0.765 \pm 0.047	0.882 \pm 0.079	0.616 \pm 0.065	0.788 \pm 0.143
	F1 score	0.778 \pm 0.023	0.549 \pm 0.001	0.757 \pm 0.035	0.837 \pm 0.127	0.600 \pm 0.100	0.775 \pm 0.124
Inference	Accuracy (%)	0.849 \pm 0.004	0.692 \pm 0.003	0.819 \pm 0.044	0.911 \pm 0.068	0.744 \pm 0.174	0.789 \pm 0.146
	F1 score	0.831 \pm 0.005	0.544 \pm 0.002	0.808 \pm 0.039	0.883 \pm 0.103	0.680 \pm 0.244	0.761 \pm 0.113

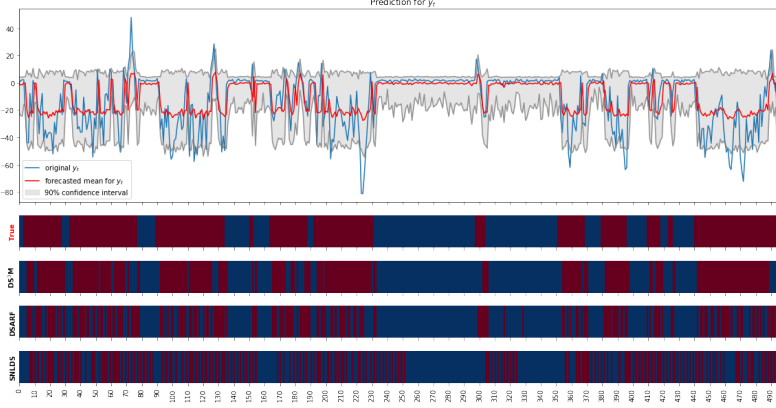
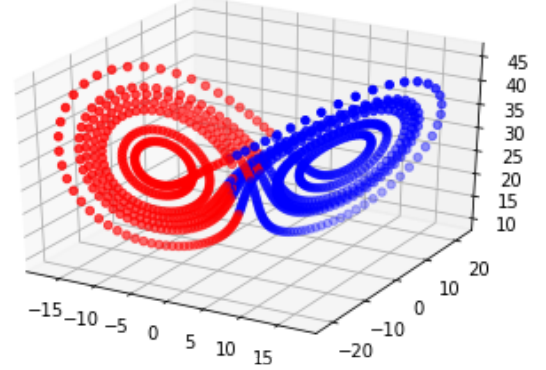
(a) Prediction for the toy example. The red color means $d_t = 0$ and the blue color means $d_t = 1$ (b) The forecasted switching variable against the true z_t .

Fig. 2: Plots for the two simulated dataset

cation of weights and factors, which fitted the assumption of the generative model of the DSARF. As for the segmentation task (inference), the DS³M also achieves the highest accuracy: 0.911 ± 0.068 (a relative improvement of 22.51% and 15.49%) and best F1 score: 0.883 ± 0.103 (a relative improvement of 29.97% and 16.06%).

We conducted additional experiments by setting the number of the switching states to 3 for this simulated dataset. The results show that it succeeds in learning to only use two states and ignore the redundant state. The redundant state has a very small average predictive probability (0.073) over the test samples, while for the other two states, the average predictive probability is 0.512 and 0.414 respectively.

B. Real data analysis

We conducted a thorough evaluation of DS³M's performance across six real-world datasets, encompassing diverse fields. These datasets are: **Sleep** Apnea, the **US unemployment** rate, **Hangzhou** metro, **Seattle** traffic and **Pacific** surface temperature, and French **electricity** demand. These datasets not only span a range of disciplines but also exhibit varying data characteristics in terms of sampling frequency and dimensionality. Here is a brief overview of each dataset:

- the **Sleep** Apnea dataset is a public physiological dataset from a patient diagnosed with sleep apnea, a medical condition in which patients intermittently stop breathing during sleep. The respiration pattern in sleep apnea can

be characterized by at least two regimes – no breathing and gasping breathing induced by reflex arousal. We use the same separation of training and testing data as in [1] and [27].

- The monthly **US Unemployment** rate¹ is one of the most important indicators of the US economy. The data are from January 1948 to March 2021 and the last 20 years are used for testing.
- The **Hangzhou** Metro dataset² consists of the incoming passenger flow of 80 metro stations in Hangzhou, China from January 1 to January 25, 2019 [27]. The passenger flow data have a temporal resolution of 10-minutes during the service hour, i.e. 108 points per day. The last 5 days are used for testing.
- The **Seattle** Traffic dataset³ contains the traffic speed from 323 loop detectors in Seattle, USA, from January 1 to January 28, 2015 [27]. It has a temporal resolution of 5-min, i.e. 288 points in a day. The last 5 days are reserved for testing.
- The **Pacific** surface temperature dataset⁴ consists of monthly surface temperatures of the Pacific for 2520 gridded spatial locations from January 1970 to December

¹US Unemployment Rate, <https://fred.stlouisfed.org/series/UNRATE>

²Hangzhou Incoming Passenger Flow, <https://tianchi.aliyun.com/competition/entrance/231708/>

³Seattle Inductive Loop Detector Dataset, <https://github.com/zhiyongc/Seattle-Loop-Data>

⁴Pacific Ocean Temperature Dataset, <http://iridl.ldeo.columbia.edu/>

TABLE III: Comparison of RMSE and MAPE on testing data. The best models are in bold. “-” indicates the model forecasts diverge to unreasonable values and are omitted.

Datasets	RMSE					MAPE (%)					
	DS ³ M	SNLDS	DSARF	SRNN	GRU	DS ³ M	SNLDS	DSARF	SRNN	GRU	
Short-term	Sleep	1201	2789	1557	1806	1264	15.46	88.06	39.25	50.8	31.17
	Unemployment	0.75	1.59	1.06	2.01	1.05	4.53	16.13	8.11	23.15	5.13
	Hangzhou	32.53	36.67	34.81	33.80	38.42	24.04	23.90	29.73	25.40	30.48
	Seattle	4.16	4.18	4.44	4.17	4.18	5.81	5.85	7.27	6.00	6.89
	Pacific	0.57	15.78	0.53	0.58	0.56	1.69	58.01	1.57	1.74	1.68
	Electricity	2971	5133	8805	3642	4784	4.58	7.79	18.64	5.34	6.60
Long-term	Hangzhou	47.50	42.83	42.28	60.89	73.18	38.20	50.6	43.65	82.81	86.61
	Seattle	4.17	4.19	-	4.17	16.93	5.81	5.86	-	5.81	27.95
	Pacific	0.72	-	0.73	0.98	0.76	2.15	-	2.29	2.99	2.22

2002 [27]. The last 5 years are used for testing.

- The French **Electricity** demand dataset contains half-hourly electricity demand in French from January 1, 2012 to December 31, 2019, which is also used in [40], [41]. The year 2019 is used for testing. For this dataset, we only have one time series and the testing data spans one year.

A summary of the data sets is provided in Table II and more details are given in the supplementary materials. We performed both short-term and long-term forecasting. For short-term prediction, we make one-step ahead forecasting with rolling windows. The models are trained on the data prior to the test data and are fixed when making forecasting for the test data. For long-term prediction, we make forecasting for all the test data sequentially standing at the start of the test data.

TABLE II: Description of the datasets

Dataset	frequency	D	T+T_test	T_test
Sleep	half a second	1	2000	1000 (500 seconds)
Unemployment	month	1	879	240 (20 years)
Hangzhou	10 mins	80	2700	540 (5 days)
Seattle	5 mins	323	8064	1440 (5 days)
Pacific	month	2520	396	60 (5 years)
Electricity	half a hour	48	2921	320 days (1 year)

a) Short-term prediction results: Table III presents the prediction results for the six datasets in terms of both MAPE (Mean Absolute Percentage Error) and RMSE (Root Mean Square Error), as defined in the supplementary materials. DS³M demonstrates superior performance across the board. Specifically, for the Sleep, Unemployment rate, Seattle, and Electricity datasets, DS³M outperforms all alternative models in terms of both RMSE and MAPE. Notably, the RMSE values exhibit relative improvements ranging from 5.0%-56.9%, 28.9%-62.8%, 0.5%-6.3%, and 18.4%-66.3% for these four datasets, while the MAPE values demonstrate reductions of 15.71%-72.60%, 0.60%-18.62%, 0.09%-1.46%, and 0.76%-14.06% against the alternative models. For the Hangzhou dataset, DS³M achieves the lowest RMSE and exhibits comparable MAPE to SNLDS (the best performing model for this dataset). For the Pacific dataset, DS³M attains competitive performance comparable to DSARF, which holds the best performance in this context.

Figure 3 visually presents the short-term predictions of the testing data along with the identified switching regimes for various datasets. For the **Sleep** dataset, DS³M segregates the time series into two distinct regimes represented by blue and red shades. Notably, the consistent red regime is found to correspond to periods when the patient experiences little to no breathing, while the blue regime corresponds to periods marked by gasping breaths. In the case of **Unemployment** rates, DS³M successfully separates the time series into two regimes. The red regimes align with times of elevated unemployment, notably during the 2009 financial crisis and the 2020 Covid-19 pandemic. Further, specific illustrations showcase values at randomly selected locations for datasets such as Hangzhou, Seattle, Pacific, and French Electricity demand. DS³M’s automated segmentation of Hangzhou traffic data into peak and non-peak hours is particularly noteworthy. In the context of the **Seattle** dataset, the red regime signifies periods of heightened traffic volatility. In the **Pacific** dataset, different regimes are associated with shifts in the time series level. For instance, at Location 0, the red regime exhibits a higher level compared to the blue regime, while the reverse is true for Location 840. Lastly, for the French **Electricity** demand dataset, the red regime is found to align predominantly with working days, while the blue regime corresponds to weekends. In general, it shows that all the predicted values trace the true values closely and the 90% confidence intervals cover most of the true values in the future.

b) Long-term prediction results: In the long-term prediction experiment, we excluded the Sleep and Unemployment datasets due to their lack of periodic patterns and high chaotic nature, making them unsuitable for long-term prediction assessment. Similarly, the Electricity dataset was omitted from the long-term prediction analysis, given its test length spanning one year, which renders long-term predictions less practical for high-frequency data across all models.

Table III showcases the long-term forecasting errors for the various datasets. Notably, DS³M exhibits superior performance in terms of RMSE for the Pacific dataset. For both Hangzhou and Pacific datasets, DS³M outperforms the alternatives in terms of MAPE. Regarding the Seattle dataset, DS³M and SRNN demonstrate comparable performance. These findings highlight DS³M’s favorable outcomes in the context

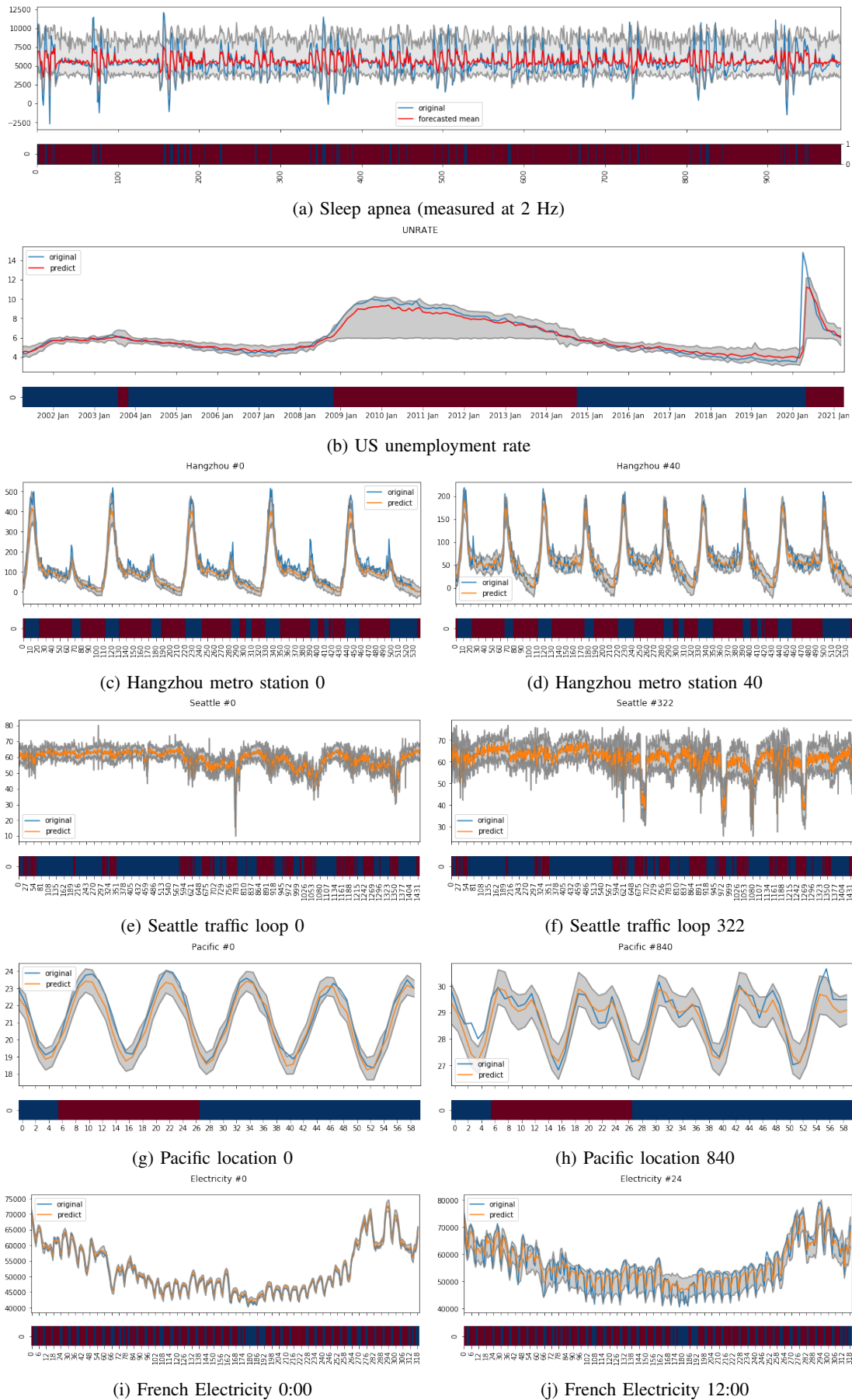


Fig. 3: Predictions of the testing data for different datasets

of long-term predictions, especially for the specific datasets mentioned.

V. CONCLUSION

We proposed the deep switching state space model (DS³M) for forecasting nonlinear time series characterized by regime switching. DS³M effectively captures these intricate dynamics by utilizing both discrete and continuous latent variables in conjunction with recurrent neural networks. This distinctive approach combines the power of deep learning with stochastic latent variable models, enabling accurate and interpretable forecasting.

A key strength of DS³M lies in its versatility across diverse datasets. The model's architecture, comprised of a recurrent neural network (RNN) and a nonlinear switching state space model (SSSM), is capable of accommodating small and large data alike. The amortized variational inference method, employed for estimation, trains both the inference and generative networks together, ensuring applicability across varying data scales. The DS³M's efficacy is demonstrated across a range of simulated and real-world datasets, showcasing its competitive performance relative to several state-of-the-art methods.

There are some limitations of the proposed model. Firstly, an open loop of the transition of the discrete variable is not considered, as we found during the experiments that current open-loop design by making the discrete latent variables always depends on the continuous latent variables and/or observations may lead to unnecessarily frequent switching of the latent variables. If there is time series with ultra-frequent regime switching behaviors, such recurrent structure may be useful. More sophisticated architecture can be designed to account for this and we leave it for future research. Secondly, it is challenging to choose the number of switching states. This is an open question in literature. Future work can use a Dirichlet prior to automatically decide the number of the switching states.

These contributions establish DS³M as a robust and adaptable tool for forecasting complex nonlinear time series, offering a bridge between the worlds of deep learning and latent variable models. As this field evolves, DS³M is positioned to enhance our ability to model and understand intricate dynamics in diverse applications.

ACKNOWLEDGMENTS

We acknowledge the financial support provided by grants A-8000828-00-00 and A-8000828-01-00 (Regime-Switching Markov Decision Process with Applications in Digital FinTech), as well as grant A-8000014-00-00 (Deep State Space Models for Non-stationary Time Series).

REFERENCES

- [1] Z. Ghahramani and G. E. Hinton, "Variational learning for switching state-space models," *Neural Computation*, vol. 12, no. 4, pp. 831–864, 2000.
- [2] E. Fox, E. B. Sudderth, M. I. Jordan, and A. S. Willsky, "Nonparametric bayesian learning of switching linear dynamical systems," in *Advances in Neural Information Processing Systems*, 2009, pp. 457–464.
- [3] G. I. Bae, W. C. Kim, and J. M. Mulvey, "Dynamic asset allocation for varied financial markets under regime switching framework," *European Journal of Operational Research*, vol. 234, no. 2, pp. 450–458, 2014.
- [4] P. François, G. Gauthier, and F. Godin, "Optimal hedging when the underlying asset follows a regime-switching markov process," *European Journal of Operational Research*, vol. 237, no. 1, pp. 312–322, 2014.
- [5] J. Durbin and S. J. Koopman, *Time series analysis by state space methods*. Oxford University Press, 2012, vol. 38.
- [6] S.-M. Chow and G. Zhang, "Nonlinear regime-switching state-space (RSSS) models," *Psychometrika*, vol. 78, no. 4, pp. 740–768, 2013.
- [7] S. Hochreiter and J. Schmidhuber, "Long short-term memory," *Neural Computation*, vol. 9, no. 8, pp. 1735–1780, 1997.
- [8] J. Chung, C. Gulcehre, K. Cho, and Y. Bengio, "Empirical evaluation of gated recurrent neural networks on sequence modeling," in *NIPS 2014 Workshop on Deep Learning*, 2014, pp. 1–9.
- [9] S. Li, X. Jin, Y. Xuan, X. Zhou, W. Chen, Y.-X. Wang, and X. Yan, "Enhancing the locality and breaking the memory bottleneck of transformer on time series forecasting," in *Advances in Neural Information Processing Systems*, 2019, pp. 5243–5253.
- [10] R. Sen, H.-F. Yu, and I. S. Dhillon, "Think globally, act locally: A deep neural network approach to high-dimensional time series forecasting," in *Advances in Neural Information Processing Systems*, 2019, pp. 4837–4846.
- [11] D. Salinas, V. Flunkert, J. Gasthaus, and T. Januschowski, "Deepar: Probabilistic forecasting with autoregressive recurrent networks," *International Journal of Forecasting*, vol. 36, no. 3, pp. 1181–1191, 2020.
- [12] A. Graves, "Generating sequences with recurrent neural networks," *CoRR*, vol. abs/1308.0850, 2013.
- [13] G. P. Zhang and M. Qi, "Neural network forecasting for seasonal and trend time series," *European Journal of Operational Research*, vol. 160, no. 2, pp. 501–514, 2005.
- [14] D. P. Kingma and M. Welling, "Auto-encoding variational bayes," in *International Conference on Learning Representations*, 2014, pp. 1–9.
- [15] D. J. Rezende, S. Mohamed, and D. Wierstra, "Stochastic backpropagation and approximate inference in deep generative models," in *International Conference on Machine Learning*, 2014, pp. 1278–1286.
- [16] J. Bayer and C. Osendorfer, "Learning stochastic recurrent networks," in *NIPS 2014 Workshop on Advances in Variational Inference*, 2014, pp. 1–9.
- [17] J. Chung, K. Kastner, L. Dinh, K. Goel, A. C. Courville, and Y. Bengio, "A recurrent latent variable model for sequential data," in *Advances in Neural Information Processing Systems*, 2015, pp. 2980–2988.
- [18] M. Fraccaro, S. K. Sønderby, U. Paquet, and O. Winther, "Sequential neural models with stochastic layers," in *Advances in Neural Information Processing Systems*, 2016, pp. 2199–2207.
- [19] R. G. Krishnan, U. Shalit, and D. Sontag, "Structured inference networks for nonlinear state space models," in *Proceedings of the AAAI Conference on Artificial Intelligence*, 2017, pp. 2101–2109.
- [20] M. Fraccaro, S. Kamronn, U. Paquet, and O. Winther, "A disentangled recognition and nonlinear dynamics model for unsupervised learning," in *Advances in Neural Information Processing Systems*, 2017, pp. 3601–3610.
- [21] E. De Bézenac, S. S. Rangapuram, K. Benidis, M. Bohlke-Schneider, R. Kurle, L. Stella, H. Hasson, P. Gallinari, and T. Januschowski, "Normalizing kalman filters for multivariate time series analysis," in *Advances in Neural Information Processing Systems*, 2020, pp. 2995–3007.
- [22] L. Girin, S. Leglaive, X. Bie, J. Diard, T. Hueber, and X. Alameda-Pineda, "Dynamical variational autoencoders: A comprehensive review," *Foundations and Trends in Machine Learning*, vol. 15, no. 1-2, pp. 1–175, 2021.
- [23] M. Schirmer, M. Eltayeb, S. Lessmann, and M. Rudolph, "Modeling irregular time series with continuous recurrent units," *CoRR*, vol. abs/2111.11344, 2021.
- [24] M. Johnson, D. K. Duvenaud, A. Wiltschko, R. P. Adams, and S. R. Datta, "Composing graphical models with neural networks for structured representations and fast inference," in *Advances in Neural Information Processing Systems*, 2016, pp. 2946–2954.
- [25] H. Dai, B. Dai, Y.-M. Zhang, S. Li, and L. Song, "Recurrent hidden semi-markov model," in *International Conference on Learning Representations*, 2016, pp. 1–17.
- [26] H. Liu, L. He, H. Bai, B. Dai, K. Bai, and Z. Xu, "Structured inference for recurrent hidden semi-markov model," in *Proceedings of the Twenty-Seventh International Joint Conference on Artificial Intelligence*, 2018, pp. 2447–2453.

- [27] A. Farnoosh, B. Azari, and S. Ostadabbas, “Deep switching auto-regressive factorization: Application to time series forecasting,” in *Proceedings of the AAAI Conference on Artificial Intelligence*, no. 8, 2021, pp. 7394–7403.
- [28] Z. Dong, B. Seybold, K. Murphy, and H. Bui, “Collapsed amortized variational inference for switching nonlinear dynamical systems,” in *International Conference on Machine Learning*, 2020, pp. 2638–2647.
- [29] S. Linderman, M. Johnson, A. Miller, R. Adams, D. Blei, and L. Paninski, “Bayesian learning and inference in recurrent switching linear dynamical systems,” in *Artificial Intelligence and Statistics*, 2017, pp. 914–922.
- [30] P. Becker-Ehmck, J. Peters, and P. Van Der Smagt, “Switching linear dynamics for variational Bayes filtering,” in *International Conference on Machine Learning*, 2019, pp. 553–562.
- [31] J. Nassar, S. Linderman, M. Bugallo, and I. M. Park, “Tree-structured recurrent switching linear dynamical systems for multi-scale modeling,” in *International Conference on Learning Representations*, 2018, pp. 1–9.
- [32] R. Kurle, S. S. Rangapuram, E. de Bézenac, S. Günnemann, and J. Gasthaus, “Deep rao-blackwellised particle filters for time series forecasting,” in *Advances in Neural Information Processing Systems*, 2020, pp. 15 371–15 382.
- [33] S. S. Rangapuram, M. W. Seeger, J. Gasthaus, L. Stella, Y. Wang, and T. Januschowski, “Deep state space models for time series forecasting,” in *Advances in Neural Information Processing Systems*, 2018, pp. 7796–7805.
- [34] T. Kipf, Y. Li, H. Dai, V. Zambaldi, A. Sanchez-Gonzalez, E. Grefenstette, P. Kohli, and P. Battaglia, “Compile: Compositional imitation learning and execution,” in *International Conference on Machine Learning*, 2019, pp. 3418–3428.
- [35] K. He, X. Zhang, S. Ren, and J. Sun, “Deep residual learning for image recognition,” in *Proceedings of the IEEE Conference on Computer Vision and Pattern Recognition*, 2016, pp. 770–778.
- [36] A. Vaswani, N. Shazeer, N. Parmar, J. Uszkoreit, L. Jones, A. N. Gomez, L. u. Kaiser, and I. Polosukhin, “Attention is all you need,” in *Advances in Neural Information Processing Systems*, 2017, pp. 1–11.
- [37] D. Geiger, T. Verma, and J. Pearl, “Identifying independence in bayesian networks,” *Networks*, vol. 20, no. 5, pp. 507–534, 1990.
- [38] R. J. Williams, “Simple statistical gradient-following algorithms for connectionist reinforcement learning,” *Machine Learning*, vol. 8, no. 3-4, pp. 229–256, 1992.
- [39] Z. Allen-Zhu, Y. Li, and Z. Song, “On the convergence rate of training recurrent neural networks,” *Advances in neural information processing systems*, vol. 32, 2019.
- [40] X. Xu, Y. Chen, Y. Goude, and Q. Yao, “Probabilistic forecasting for daily electricity loads and quantiles for curve-to-curve regression,” *Applied Energy*, vol. 301, pp. 1–14, 2021.
- [41] H. Cho, Y. Goude, X. Brossat, and Q. Yao, “Modeling and forecasting daily electricity load curves: A hybrid approach,” *Journal of the American Statistical Association*, vol. 108, no. 501, pp. 7–21, 2013.